Ultrafast heterogeneous electron transfer reactions: Comparative theoretical studies on time- and frequency-domain data

Luxia Wang
Institut für Physik, Humboldt-Universität zu Berlin, Newtonstraße 15, D-12489 Berlin, Germany

Frank Willig
Hahn-Meitner-Institut, Abteilung Dynamik von Genzflächenreaktionen, Glienicker Strasse 100, 14109 Berlin, Germany

Volkhard May[a)]
Institut für Physik, Humboldt-Universität zu Berlin, Newtonstraße 15, D-12489 Berlin, Germany

(Received 29 August 2005; accepted 1 November 2005; published online 6 January 2006)

Recent theoretical studies on linear absorption spectra of dye-semiconductor systems [perylene attached to nanostructured TiO_2, L. Wang *et al.*, J. Phys. Chem. B **109**, 9589 (2005)] are extended here in different respects. Since the systems show ultrafast photoinduced heterogeneous electron transfer the time-dependent formulation used to compute the absorbance is also applied to calculate the temporal evolution of the sub-100 fs charge injection dynamics after a 10 fs laser-pulse excitation. These studies complement our recent absorption spectra fit for two perylene bridge-anchor group TiO_2 systems. Moreover, the time-dependent formulation of the absorbance is confronted with a frequency-domain description. The latter underlines the central importance of the self-energy caused by the coupling of the dye levels to the semiconductor band continuum. The used model is further applied to study the effect of different parameters such as (1) the dependence on the reorganization energies of the involved intramolecular transitions, (2) the effect of changing the transfer integral which couples the excited dye state with the band continuum, and (3) the effect of the concrete form of the semiconductor band density of states. Emphasis is also put on the case where the charge injection level of the dye is near or somewhat below the band edge. This nicely demonstrates the change from a structureless absorption to a well-resolved vibrational progression including characteristic shifts of the absorption lines which are a direct measure for the dye-semiconductor coupling. © *2006 American Institute of Physics*. [DOI: 10.1063/1.2140711]

I. INTRODUCTION

Although there are practical device applications of heterogeneous electron transfer (HET) reactions, e.g., in nanohybrid systems,[1–6] the exploration of the unique properties of such transfer processes is an interesting topic in its own rights. This is particularly the case if the transfer takes place on a 10 fs time scale, just offering an example for an ultrafast electron transfer process. The present paper continues a series of theoretical studies (cf. Refs. 7–11) on HET with particular emphasis on the perylene-TiO_2 system. This system is well suited for a systematic study of photoinduced ultrafast HET since the first excited perylene state is energetically positioned about 1 eV above the band edge, thus realizing a midband charge injection situation. Introducing different bridge-anchor groups the transfer coupling initiating HET can be tuned from a strong-coupling situation (with charge injection times of 10 fs) to weaker-coupling strength [with charge injection times of up to 1 ps (Ref. 12)].

In our earlier papers we developed a charge injection model which fully accounts for (1) the continuum of the TiO_2 conduction-band states, which (2) describes the transfer coupling between the excited dye state and the band continuum beyond any perturbation theory, and which (3) includes intraperylene vibrational motion (via a perylene in-plane C–C stretching vibration with a quantum energy of 1370 cm^{-1}). Furthermore, the model could be well adopted to different perylene bridge-anchor group TiO_2 systems. This has been achieved by a systematic fit of linear absorbance spectra for the perylene bridge-anchor group system in a solvent and also when attached to TiO_2 nanoparticles.

In the present paper we will continue these studies concentrating on the effects of different parameters. We will demonstrate the dependence of the absorbance on the reorganization energies of the involved intramolecular transitions. Moreover, the effect is studied of changing the transfer integral which couples the excited dye state to the band continuum. It is investigated how the concrete form of the semiconductor band density of states (DOS) influences the absorbance. These frequency-domain results are made complete by some simulations on the charge injection dynamics not present in Ref. 11. Emphasis is also put on the case where the charge injection level of the dye is near or somewhat below the band edge.

The paper is organized as follows. In Sec. II we shortly introduce the model the simulations are based on. Section III concentrates on time-domain methods either to simulate charge injection dynamics or to compute the frequency-

[a)]Electronic mail: may@physik.hu-berlin.de

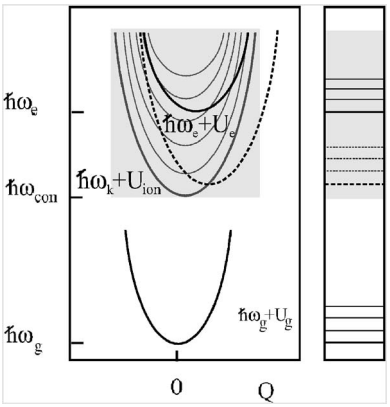

FIG. 1. Scheme of PES according to the used model Hamiltonian [Eq. (1)] (left part: the gray box indicates the continuum of band states). The position of the excited-state PES drawn by a full line is typical for perylene on TiO_2 whereas that drawn by a dashed curve resembles the near-band-edge position. The right part shows related electron-vibrational levels of the single-mode dye model (the thin lines display excited vibrational levels).

dependent absorbance. Since charge injection takes place in a 50 fs time region but, for example, intramolecular vibrational energy redistribution (IVR) on a much larger one the studies are exclusively based on a solution of the time-dependent Schrödinger equation, negelcting any effect of energy dissipation.

This treatment is complemented in Sec. IV by frequency-domain computations. Besides a formula for an exact calculation of linear absorption spectra we also demonstrate the computation of the decay of the excited dye state into the band continuum. All approaches are illustrated by different simulations in Secs. V and VI. The last one puts emphasis on the case of a near-band-edge injection position in the dye. Although this has been done for a fictitious system by using in part parameters for the perylene TiO_2 system we believe that future experiments will confirm the obtained behavior. The paper ends with some concluding remarks.

II. THE MODEL

In order to discuss HET reactions we use a model already applied in our former studies (cf. Fig. 1).[7–11] It is based on the following electron-vibrational Hamiltonian expanded with respect to the electronic states involved:

$$H_{\mathrm{M\text{-}S}} = \sum_{a=g,e,\mathbf{k}} (\hbar\varepsilon_a + H_a)|\varphi_a\rangle\langle\varphi_a| + \sum_{\mathbf{k}} (V_{\mathbf{k}e}|\varphi_{\mathbf{k}}\rangle\langle\varphi_e| + \mathrm{h.c.}). \quad (1)$$

According to the diabatization the expression includes the ground and the first excited state of the dye, φ_g and φ_e, respectively, as well as the huge number of states $\varphi_{\mathbf{k}}$ which belong to the conduction band of the semiconductor. The use of a $\mathbf{k}$ vector is representative for the many conducting states. One may distinguish between more bulklike and more surfacelike states. The injection dynamics are only slightly modified if some of the actual acceptor states are surface resonances. Therefore, occurrence of the latter will be neglected in the present paper, and we will concentrate here on a common class of states with the DOS defined below. The energy levels related to the states introduced so far are denoted as $\hbar\varepsilon_g$, $\hbar\varepsilon_e$, and $\hbar\varepsilon_{\mathbf{k}}$. The latter is written as $\omega_{\mathrm{con}} + \omega_{\mathbf{k}}$, with the lower band edge ω_{con} and $\omega_{\mathbf{k}}$ running over the conduction band with width $\Delta\omega_{\mathrm{con}}$. All levels are understood as given by the minima of the related potential-energy surfaces (PESs) plus the zero-point vibrational energy. Thus, the spectrum of the vibrational Hamiltonian starts at zero energy. H_g and H_e denote those for the electronic ground state and the first excited state of the dye, respectively, and H_{ion} is the one of the ionized dye if charge injection into the conduction band took place. The related eigenvalues and vibrational wave functions are $\hbar\omega_{aM}$ and χ_{aM}, respectively (M denote the vibrational quantum numbers).

Charge injection from φ_e into the manifold of states $\varphi_{\mathbf{k}}$ is realized by the transfer coupling $V_{\mathbf{k}e}$ (which should not depend on vibrational coordinates). For the following it is customary to change from the $\mathbf{k}$ dependence of the band energy and the transfer coupling to a continuous frequency dependence by introducing the DOS,

$$\mathcal{N}(\Omega) = \sum_{\mathbf{k}} \delta(\Omega - \omega_{\mathbf{k}}), \quad (2)$$

and by replacing $V_{e\mathbf{k}}$ by $V_e(\Omega)$.

Optical excitation should take place exclusively in the dye molecule between the ground and the excited state described by the dipole operator,

$$\hat{\mu} = \mathbf{d}_{eg}|\varphi_e\rangle\langle\varphi_g| + \mathrm{h.c.}\ . \quad (3)$$

The transition-dipole matrix element is denoted by $\mathbf{d}_{eg}$.

III. TIME-DOMAIN DESCRIPTION

We start our consideration with a time-dependent description of the system. This was the main focus of our foregoing studies.[7–10] They dealt with the photoinduced dynamics concentrating on a 100 fs time window where it is reasonable to neglect any relaxational effect. Therefore, it was possible to simply propagate the time-dependent Schrödinger equation related to the Hamiltonian introduced in Eq. (1). To solve the Schrödinger equation we carry out an expansion with respect to the diabatic electron-vibrational states $\chi_{aM}\varphi_a$ and obtain

$$|\Psi(t)\rangle = \sum_{aM} C_{aM}(t)|\chi_{aM}\rangle|\varphi_a\rangle. \quad (4)$$

Populations of the dye states follow as $P_g = \Sigma_M |C_{gM}(t)|^2$ and $P_e = \Sigma_M |C_{eM}(t)|^2$. That of the ionized state my be obtained from $P_{\mathrm{ion}}(t) = 1 - P_g - P_e$. The given state expansion is fairly standard except for the presence of the band continuum leading to a continuous set $C_{\mathbf{k}M}(t)$ of expansion coefficients. We will tackle this problem as described in. Refs. 7–11. Therefore, the $\mathbf{k}$ dependence of the $C_{\mathbf{k}M}(t)$ is replaced by a frequency dependence leading to the quantities $C_M(\omega;t)$. They will be expanded by the functions $u_r(\omega)$ forming an orthogonal set. The latter is complete over the energy range of the conduction band, here characterized by the frequency interval $[0, \Delta\omega_{\mathrm{con}}]$ (from the lower to the upper conduction band edge). This allows us to write

$$C_M(\omega;t) = \sum_r u_r(\omega) C_M^{(r)}(t). \tag{5}$$

An appropriate truncation of the infinite sum leads to a finite set of expansion coefficients $C_M^{(r)}(t)$. As already demonstrated in Refs. 8 and 9 the expansion with respect to the functions $u_r(\omega)$ (substantiated by Legendre polynomials) reduces the effort to account for the continuous band energy enormously (compared to a naive discretization of the band energies).

Next, we present the set of coupled equations of motion for the expansion coefficients C_{aM} introduced in Eq. (4). Those equations related to the conduction-band continuum are rewritten using Eq. (5). The equations take the following forms:

$$\frac{\partial}{\partial t} C_{gM}(t) = -i(\varepsilon_g + \omega_{gM}) C_{gM}(t) + \frac{i}{\hbar} \mathbf{E}(t) \mathbf{d}_{ge} \sum_N \langle \chi_{gM} | \chi_{eN} \rangle C_{eN}(t), \tag{6}$$

$$\frac{\partial}{\partial t} C_{eM}(t) = -i(\varepsilon_e + \omega_{eM}) C_{eM}(t) + \frac{i}{\hbar} \mathbf{E}(t) \mathbf{d}_{eg} \sum_N \langle \chi_{eM} | \chi_{gN} \rangle C_{gN}(t) - \frac{i}{\hbar} \sum_p \sum_N \langle \chi_{eM} | \chi_{\text{ion } N} \rangle \langle \mathcal{N} V_e u_p \rangle_\omega C_N^{(p)}(t), \tag{7}$$

and

$$\frac{\partial}{\partial t} C_M^{(r)}(t) = -i(\omega_{\text{con}} + \omega_{\text{ion } M}) C_M^{(r)}(t) - i \sum_p \langle \omega u_r u_p \rangle_\omega C_M^{(p)}(t) - \frac{i}{\hbar} \sum_N \langle u_r V_e \rangle_\omega \langle \chi_{\text{ion } M} | \chi_{eN} \rangle C_{eN}(t). \tag{8}$$

The bracket $\langle \cdots \rangle_\omega$ denotes frequency integration according to the relation

$$\langle u_r u_p \rangle_\omega \equiv \int_0^{\omega_{\max}} d\omega u_r(\omega) u_p(\omega) = \delta_{r,p}. \tag{9}$$

The relation also indicates orthonormalization of the functions $u_r(\omega)$. The expressions $\langle \mathcal{N} V_e u_p \rangle_\omega$ and $\langle u_r V_e \rangle_\omega$ account for the frequency dependence of the DOS and the transfer coupling.

For the concrete calculations we used a particular realization of the orthonormal set u_r. It is given by the Legendre polynomials P_r according to the identification

$$u_r(\omega) = \sqrt{\frac{2r+1}{\omega_{\max}}} P_r(x(\omega)), \tag{10}$$

with

$$x(\omega) = \frac{2\omega}{\omega_{\max}} - 1. \tag{11}$$

The necessary number of the polynomials did not exceed 200 whereas the upper vibrational number was $M=22$.

Once the time-dependent Schrödinger equations related to ultrafast HET have been solved different quantities of interest can be computed. We concentrate here on the time-dependent formulation of the cw-absorption coefficient, an approach which has been also used recently in Ref. 11. A particular aim here will be a univocal description based on Green's operator projected on the injecting level. This approach will also bridge the gap to quantities determined in the frequency domain.

A. The absorption coefficient

A short reminder of the general expression of the linear absorption $\alpha(\omega)$ is given in Appendix B. Neglecting non-Condon effects $\alpha(\omega)$ is mainly determined by the combined DOS $\mathcal{D}_{\text{abs}}$ which refers to ground-state–excited-state transition in the dye. For the following computations we will concentrate on a situation where only the vibrational ground state χ_{g0} of the electronic ground state is populated (low temperatures or exclusively high-frequency vibrational modes or both). Then, Eq. (B4) reduces to

$$\mathcal{D}_{\text{abs}}(\omega) = -\frac{1}{\pi\hbar} \text{Im} \int dt e^{i(\omega+\varepsilon_g)t} \langle \chi_{g0} | \hat{G}_e(t) | \chi_{g0} \rangle. \tag{12}$$

Note the introduction of Green's operator projected onto the injecting level ($\hat{\Pi}_e = |\varphi_e\rangle\langle\varphi_e|$),

$$\hat{G}_e(t) = -i\Theta(t) \hat{\Pi}_e e^{-iH_{\text{M-S}}t/\hbar} \hat{\Pi}_e. \tag{13}$$

This formula together with that for $\mathcal{D}_{\text{abs}}$ demonstrates that the state vector $|\chi_{g0}\rangle|\varphi_e\rangle$ has to be propagated under the action of the complete Hamiltonian $H_{\text{M-S}}$ [Eq. (1)] (the absence of any ground-state–excited-state coupling in $H_{\text{M-S}}$, however, eliminates any ground-state contribution). We introduce the expansion [Eq. (4)] with respect to the electron-vibrational states $|\chi_{aM}\rangle|\varphi_a\rangle$ (with a restricted to e and $\mathbf{k}$) and with the initial condition,

$$C_{aM}(0) = \delta_{a,e} \langle \chi_{eM} | \chi_{g0} \rangle. \tag{14}$$

According to this treatment one obtains

$$\langle \chi_{g0} | \hat{G}_e(t) | \chi_{g0} \rangle = -i\Theta(t) \sum_M \langle \chi_{g0} | \chi_{eM} \rangle C_{eM}(t). \tag{15}$$

Before presenting some results based on the use of this formula we discuss first the computation of some frequency-domain quantities. In particular, this will offer a simple picture of the influence of the excited dye state conduction-band coupling which is rather hidden in the time-dependent description.

IV. FREQUENCY-DOMAIN DESCRIPTION

Again we make continuous use of Green's operator projected onto the injecting level φ_e [Eq. (13)]. Here, its vibrational matrix elements will be computed directly what, in particular, gives a lucid formula for the absorbance. Details on Green's operator may be found in Appendix A.

A. Decay into the band continuum

Let us first calculate the decay of the population $P_{eM}(t)$ of an excited dye electron-vibrational state $\chi_{eM}\varphi_e$ upon charge injection starting at $t=0$. Using Green's operator [Eq. (13)] one immediately obtains

$$P_{eM}(t) = \Theta(t)|\langle\varphi_e\chi_{eM}|\hat{G}_e(t)|\chi_{eM}\varphi_e\rangle|^2 \equiv \left|\int \frac{d\omega}{2\pi} G_{e,MM}(\omega)\right|^2. \tag{16}$$

The latter expression contains electron-vibrational matrix elements of $\hat{G}_e(t)$ which can be determined by solving Eq. (A3). As a main ingredient the self-energy due to the coupling of the excited dye level to the band continuum appears

$$\Sigma(\omega) = \frac{1}{\hbar^2}\sum_{\mathbf{k}} \frac{|V_{\mathbf{k}e}|^2}{\omega - \varepsilon_{\mathbf{k}} + i\epsilon}. \tag{17}$$

The imaginary part of $\Sigma(\omega)$ will be denoted as

$$-\operatorname{Im}\Sigma(\omega) = \Gamma(\omega) = \frac{\pi}{\hbar^2}\mathcal{N}(\omega)|V_e(\omega)|^2, \tag{18}$$

where we introduced the DOS [Eq. (2)].

In the general case an analytical expression for $P_{eM}(t)$ [Eq. (16)] is hardly obtainable. Applying, however, the wide-band approximation (where the frequency dependence of the self-energy is neglected) the standard expression

$$P_{eM}(t) = e^{-k_{\mathrm{HET}}t} \tag{19}$$

follows. The rate of HET is obtained as

$$k_{\mathrm{HET}} = -2\operatorname{Im}\bar{\Sigma} \equiv 2\bar{\Gamma} = \frac{2\pi}{\hbar^2}\bar{\mathcal{N}}|\bar{V}_e|^2, \tag{20}$$

with the mean (frequency-averaged) DOS $\bar{\mathcal{N}}$ and the mean transfer coupling $\bar{V}_e$. Note that this wide-band approximation suppresses any vibrational contributions.

B. The absorption coefficient

To gain some further insight into the influence of the dye-semiconductor coupling on the absorption spectrum, next, we will present an alternative description of the absorbance to that of the preceding section. We start with Eq. (12) but generalized to finite temperatures. Since electronic ground-state vibrational matrix elements of the Green's operator [Eq. (13)] appear we have to insert the vibrational completeness relation referring to the excited dye state. This leads to the proper matrix elements of Green's operator and we may write

$$\mathcal{D}_{\mathrm{abs}}(\omega) = -\frac{1}{\pi\hbar}\sum_N f(\hbar\omega_{gN})\operatorname{Im}\int dt e^{i(\omega+\varepsilon_g+\omega_{gN})t} \times \sum_{K,L}\langle\chi_{gN}|\chi_{eK}\rangle G_{e,KL}(t)\langle\chi_{eL}|\chi_{gN}\rangle. \tag{21}$$

After carrying out the time integral we arrive at

$$\mathcal{D}_{\mathrm{abs}}(\omega) = -\frac{1}{\pi\hbar}\sum_{N,K,L} f(\hbar\omega_{gN})\operatorname{Im}(\langle\chi_{gN}|\chi_{eK}\rangle \times G_{e,KL}(\omega+\varepsilon_g+\omega_{gN})\langle\chi_{eL}|\chi_{gN}\rangle). \tag{22}$$

The matrix elements $G_{e,KL}$ have to be computed according to Eq. (A3). Of course this scheme is useful only in such situations where only a selected number of vibrational coordinates have to be considered.

In the wide-band approximation, Eq. (22) for the combined DOS reduces to [cf. Eq. (A5)]

$$\mathcal{D}_{\mathrm{abs}}(\omega) = \frac{1}{\pi\hbar}\sum_{N,K} f(\hbar\omega_{gN})|\langle\chi_{gN}|\chi_{eK}\rangle|^2 \times \frac{\operatorname{Im}\bar{\Sigma}}{(\omega-\varepsilon_{eg}-\omega_{eK,gN}-\operatorname{Re}\bar{\Sigma})^2+(\operatorname{Im}\bar{\Sigma})^2}. \tag{23}$$

Note the introduction of transition frequencies $\varepsilon_{eg}=\varepsilon_e-\varepsilon_g$ and $\omega_{eK,gN}=\omega_{eK}-\omega_{gN}$. As a result, the combined DOS follows as an expression with Lorentzian line shapes for every ground-state–excited-state transition. The broadening is originated by the imaginary part of the self-energy [cf. Eqs. (17) and (18)], whereas the real part of the self-energy induces a shift of the transition frequencies and reads ($\mathcal{P}$ indicates that the principle part of the integral has to be taken)

$$\operatorname{Re}\Sigma(\omega) = \frac{1}{\hbar^2}\int d\Omega\mathcal{P}\frac{\mathcal{N}(\Omega)|V_e(\Omega)|^2}{\omega-\Omega}. \tag{24}$$

The frequency-independent quantity $\operatorname{Re}\bar{\Sigma}$ appearing in Eq. (23) is obtained in replacing ω by a fixed frequency ω_0, for example, the actual transition frequency. Once ω_0 is positioned around the lower conduction band edge ω_{con} the integrand is mainly negative and we expect a negative value of $\operatorname{Re}\bar{\Sigma}$. This negative shift of the transition frequencies becomes smaller when moving ω_0 into a midband position (positive contributions to the overall Ω integral increase). Such a behavior is confirmed by our numerical calculation based on the time-domain formulation of the absorbance and will be discussed in detail below.

The described behavior of the absorption coefficient reflects the Fano effect caused by the coupling of the excited dye electron-vibrational levels to the conduction-band continuum. However, when leaving the wide-band approximation the Fano effect entering Eq. (22) is hidden by Green's operator matrix elements.

V. THE REFERENCE CASE: PERYLENE ON TiO_2

The following numerical results address our recent studies on the perylene TiO_2 system[11] where different parameters could be deduced. All these considerations will be confronted by computations for those systems where the charge injection level is closer to the lower semiconductor conduction band edge. In Ref. 11 absorption spectra for perylene attached with different bridge-anchor groups to the TiO_2 surface have been analyzed in detail. We concentrate here on the strong-coupling case realized by a carboxylic acid bridge-anchor group (–COOH) and on the case of a somewhat weaker coupling given by the proprionic acid bridge-anchor

TABLE I. Parameters of the DTB–Pe–COOH system at the TiO_2 surface.

$\hbar\varepsilon_e$	2.79 eV
$\hbar\omega_{\text{vib}}$	0.16 eV
λ_{eg}, (Q_e-Q_g)	0.116 eV,(1.7)
$\hbar\gamma$	0.062 eV
$\hbar\varepsilon_{\text{con}}$	1.79 eV
$\hbar\Delta\omega_{\text{con}}$	6.0 eV
$\hbar\bar{\Gamma}$	0.094 eV
$\bar{V}_e$ $(\bar{\mathcal{N}}/\hbar)$	0.122 eV,(2/eV)
$\lambda_{\text{ion }e}$, $(Q_{\text{ion}}-Q_e)$	0.014 eV,(−0.6).

group $[-(CH_2)_2-COOH$, for more details see also Ref. 11]. In any case the use of a single vibrational coordinate referring to the in-plane C–C stretching vibration of perylene was sufficient for simulating the spectra. This allows to denote the PES involved as $(a=g,e$, ion)

$$U_a(Q)=\hbar\omega_{\text{vib}}\left(\tfrac{1}{4}(Q-Q_a)^2+\tfrac{1}{2}\right), \tag{25}$$

with the vibrational frequency ω_{vib} common to all considered electronic states (for the concrete values see the Tables I and II). The notation includes the zero-point energy and is based on the use of a dimensionless coordinate Q (Q_a denote the respective equilibrium positions). Reorganization energies for transitions among the states simply follow as

$$\lambda_{ab}=\frac{\hbar\omega_{\text{vib}}}{4}(Q_a-Q_b)^2. \tag{26}$$

They coincide with half of the respective Stokes shift.

Once the line broadening $\bar{\Gamma}$ [Eq. (20)] is determined one may deduce the mean transfer integral $\bar{V}_e$. In order to do this we used the density-functional theory (DFT) calculations on perylene TiO_2 systems of Refs. 13 and 14 to estimate the mean DOS $\mathcal{N}$. While a determination of the transfer coupling requires a so-called diabatization (the used DFT calculations only offer common dye TiO_2 nanoparticle levels), $\mathcal{N}$ is directly obtained from calculations neglecting the presence of the dye on the nanoparticle. These calculations suggest as a rough estimate a Gaussian-type DOS extending across the conduction band (with a width of about 6 eV). The absolute value can be obtained by counting the number of TiO_2 levels per eV. All this leads to rather reasonable values of $\bar{V}_e$ as given in Tables I and II.

TABLE II. Parameters of the DTB−Pe−$(CH_2)_2$−COOH system at the TiO_2 surface. (For the solvent case we have $\lambda_{eg}=0.123$ eV.)

$\hbar\varepsilon_e$	2.79 eV
$\hbar\omega_{\text{vib}}$	0.17 eV
λ_{eg}, (Q_e-Q_g)	0.187 eV,(2.1)
$\hbar\gamma$	0.058
$\hbar\varepsilon_{\text{con}}$	1.79 eV
$\hbar\Delta\omega_{\text{con}}$	6.0 eV
$\hbar\bar{\Gamma}$	0.0213
$\bar{V}_e$ $(\bar{\mathcal{N}}/\hbar)$	0.058 eV,(2/eV)
$\lambda_{\text{ion }e}$, $(Q_{\text{ion}}-Q_e)$	0.014 eV,(−0.6)

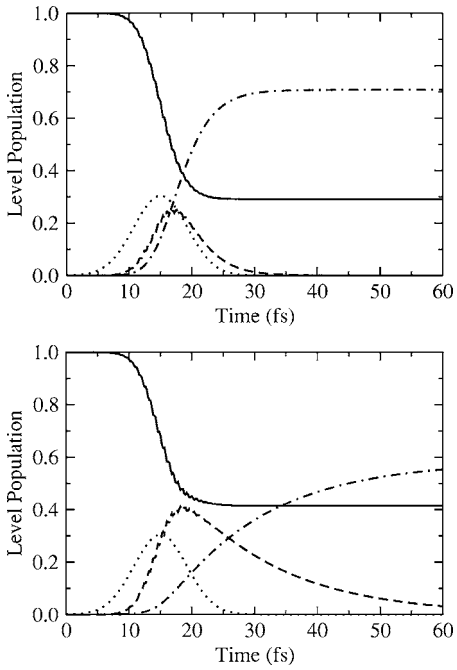

FIG. 2. Electronic level population after a 10 fs (FWHM) laser pulse excitation. Upper panel: the DTB–Pe–COOH system (for parameters see Table I), lower panel: the DTB–Pe–$(CH_2)_2$–COOH system (for parameters see Table II), solid line: ground-state population P_g of the dye, dashed line: excited-state population P_e of the dye, dashed-dotted line: population P_{ion} of the ionized dye (what equals the total conduction band population), and dotted line: laser-pulse envelope (in a.u.).

A. Charge injection dynamics

Charge injection dynamics related to the two bridge-anchor groups described in the preceding section are displayed in Fig. 2. The calculations are the result of a complete solution of Eqs. (6)–(8), starting at the vibrational ground state χ_{g0} of the electronic ground state and including a laser field of 10 fs duration [full width at half maximum (FWHM)]. Moreover, the wide-band approximation has been used, thus, replacing $\langle\mathcal{N}V_e u_p\rangle_\omega$ and $\langle u_r V_e\rangle_\omega$ in Eqs. (7) and (8) by $\delta_{p,0}\bar{\mathcal{N}}\bar{V}_e$ and $\delta_{r,0}\bar{V}_e$, respectively. In the strong-coupling case the excited-state population P_e follows the laser-pulse envelope accompanied by a direct charge transfer into the conduction-band continuum. The respective overall band population is identical to the population of the ionized dye state P_{ion}. Here, one may consider the laser-pulse excitation as a direct population of the semiconductor states. In the other case with a weaker coupling the excited-state population starts to decay into the band continuum when the laser-pulse excitation is over, indicating the separation of excited-state preparation and charge injection. All the parameters used for the simulations may be found in the Tables I and II.

B. Linear absorption spectra

Next let us turn to the discussion of the absorption spectra. Results of respective calculations together with the measured absorbances can be found in the Figs. 3 and 4. The measured solvent spectra show a vibrational progression which has been related to a perylene in-plane C–C stretching vibration with a quantum energy of 1370 cm^{-1}.[11] The 0-0

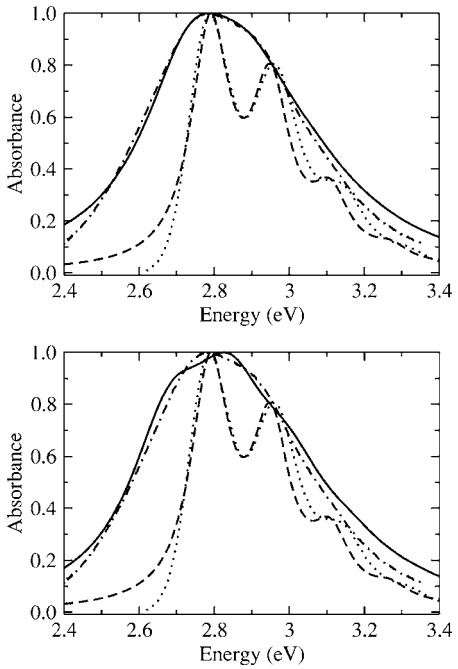

FIG. 3. Rescaled linear absorption spectrum of the DTB–Pe–COOH system. Upper panel: parameters according to Table I, lower panel: surface attached case with some altered parameters ($\hbar\varepsilon_e$=2.72 eV, λ_{eg}=0.187 eV, and $\hbar\bar{\Gamma}$ =0.069 eV), dotted lines: experimental data for the system in the solvent, dashed-dotted lines: experimental data for the system adsorbed at a TiO_2 surface, dashed lines: calculated data for the system in the solvent, and full lines: calculated data for the system adsorbed at a TiO_2 surface. [While the upper spectra give the best coincidence between measured and simulated data the lower spectra are more consistent with other studied perylene bridge-anchor groups (see Ref. 11).]

transition as well as the 0-1, 0-2, and 0-3 transitions are clearly resolved. The solvent spectra have been used to fix some internal perylene parameters (energetic position of the excited state, vibrational energy, and reorganization energy accompanying the excitation and overall dephasing rate).

These spectra as well as those for the case of perylene attached to TiO_2 could be rather well reproduced. For their computation we mainly applied Eq. (12) for the combined DOS (time-domain formulation) but also Eq. (23) (frequency-domain formulation). In the first case we had to

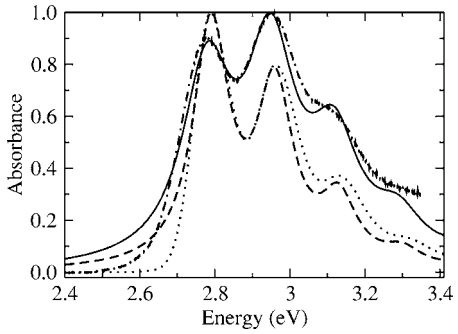

FIG. 4. Rescaled linear absorption spectrum of the DTB–Pe–$(CH_2)_2$–COOH system. Dotted lines: experimental data for the system in the solvent, dashed-dotted lines: experimental data for the system adsorbed at a TiO_2 surface, dashed lines: calculated data for the system in the solvent, and full lines: calculated data for the system adsorbed at a TiO_2 surface (for the used parameters see Table II).

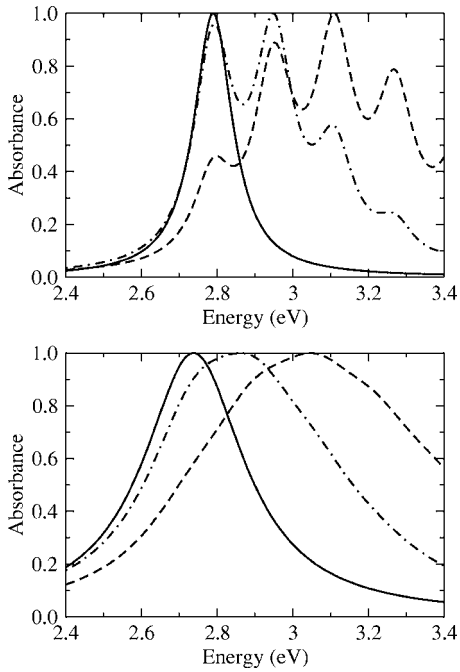

FIG. 5. Rescaled linear absorption spectrum of the DTB–Pe–COOH system in a solvent (upper panel) and attached to the TiO_2 surface (lower panel). The reorganization energy λ_{eg} is varied via a change of Q_e-Q_g [cf. Eq. (26)]. Solid line: $Q_e-Q_g=0$, dashed-dotted line: $Q_e-Q_g=2$ (λ_{eg}=0.16 eV), and dashed line: $Q_e-Q_g=3$ (λ_{eg}=0.36 eV; for other parameters see Table I).

propagate the Eqs. (7) and (8), what has been done similar to those computations carried out on the charge injection dynamics presented beforehand.

Figure 3 shows two possible fits of the strong-coupling case. The fit of the lower panel has been suggested in Ref. 11 and could be rather well arranged in the observed behavior of a sequence of four different bridge-anchor groups. Here, we prefer the fit presented in the upper panel of Fig. 3 which shows better agreement with the experimental data and does not require a change of the excited perylene level.

When applying the direct frequency-domain formulation according to Eq. (23) for the absorbance (combined DOS) we concentrate on the strong-coupling case as displayed in the upper panel of Fig. 3. The used values of $\bar{\Gamma}$ follow from the respective calculations. To achieve complete agreement with the time-domain computations, additionally, a transition frequency shift originated by $\hbar\,\mathrm{Re}\,\bar{\Sigma}$ of about −0.05 eV has to be introduced. Interestingly, the combined effect of strong line broadening and a redshift of the transition frequencies gives the impression that the absorbance peak for the case of perylene attached to TiO_2 stays at the same position as that for perylene in a solvent.

C. Dependence of the absorbance on different parameters

The results shown in the Figs. 3 and 4 are next illustrated by demonstrating their dependence on different parameters. Figure 5 shows for DTB–Pe–COOH on TiO_2 (strong-coupling case) how the absorbance changes if the reorganization energy λ_{eg} for the transition from the ground to the excited perylene state [cf. Eq. (26)] is altered. If we consider

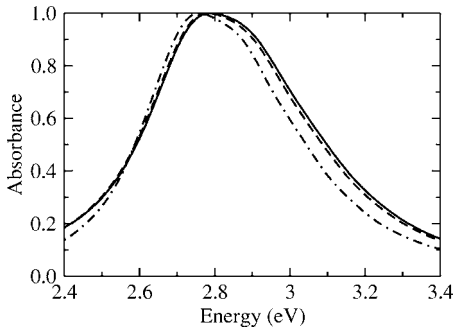

FIG. 6. Rescaled linear absorption spectrum of the DTB–Pe–COOH system adsorbed at the TiO_2 surface. The reorganization energy $\lambda_{\text{ion }e}$ for the cation formation accompanying the charge injection process is varied via a change of $Q_{\text{ion}}-Q_e$ [cf. Eq. ((26))]. Solid line: $Q_{\text{ion}}-Q_e=0$, dashed line: $Q_{\text{ion}}-Q_e=1$ ($\lambda_{\text{ion }e}=0.04$ eV), and dashed-dotted line: $Q_{\text{ion}}-Q_e=3$ ($\lambda_{\text{ion }e}=0.36$ eV; for other parameters see Table I).

the dye in a solvent an increase of λ_{eg} shifts the oscillator strength into higher levels of the vibrational progression. This behavior remains if the dye is coupled to the semiconductor but in the present case without a resolution of the different vibrational contributions. In contrast, the dependence on the reorganization energy for the excited-state–ionized-state transition is less pronounced, as shown in Fig. 6.

The loss of resolution of the vibrational progression with an increase of $\bar{\Gamma}$ [respective $\bar{V}_e$, cf. Eq. (20)] is demonstrated in Fig. 7. The results have been obtained in applying Eqs. (12) and (15) based on a solution of the time-dependent Schrödinger equation of the charge injection process. As already stated in relation to Fig. 3 the combined effect of level broadening and a redshift results in a rather constant absorbance peak position when increasing $\bar{V}_e$.

Concluding these considerations, we underline that the drastic changes of the spectra upon changing λ_{eg} and $\bar{\Gamma}$ indicate that the fit of the measured data (within the single vibrational coordinate description) has to be considered as rather univocal.

D. Influence of the conduction-band DOS

To study the influence of the frequency dependence of the DOS let us take the following form:

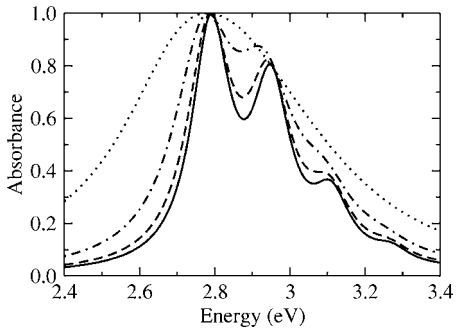

FIG. 7. Rescaled linear absorption spectrum of the DTB–Pe–COOH system adsorbed at the TiO_2 surface with the level-broadening $\bar{\Gamma}$ varied. Solid line: $\hbar\bar{\Gamma}=0$ (solvent case of Fig. 3), dashed line: $\hbar\bar{\Gamma}=0.009$ eV, dashed-dotted line: $\hbar\bar{\Gamma}=0.034$ eV, and dotted line: $\hbar\bar{\Gamma}=0.138$ eV (for other parameters see Table I).

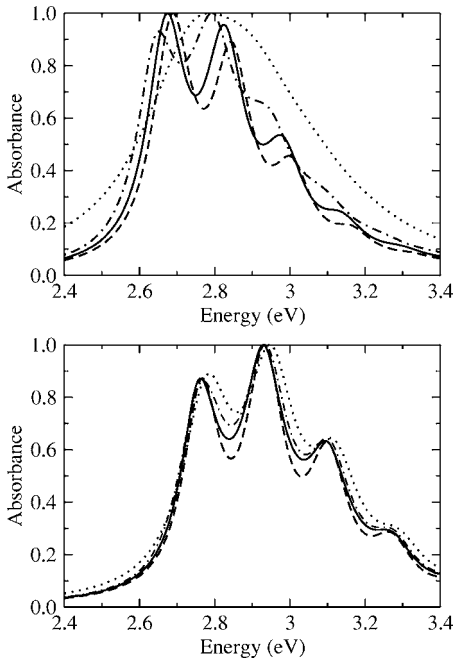

FIG. 8. Rescaled linear absorption spectra of the DTB–Pe–COOH system at the TiO_2 surface (upper panel, dotted line) and for DTB–Pe–$(CH_2)_2$–COOH (lower panel, dotted line) based on the use of a constant DOS $\bar{\mathcal{N}}$ (and with lower band edge at 1.79 eV). To indicate the effect of an injection position closer to the band edge than in TiO_2 curves with an increasing band-edge energy $\hbar\omega_{\text{con}}$ are also shown. Dashed-dotted line: $\hbar\omega_{\text{con}}=2.69$ eV, solid line: $\hbar\omega_{\text{con}}=2.79$ eV, and dashed line: $\hbar\omega_{\text{con}}=2.89$ eV.

$$\mathcal{N}(\omega)=\nu\sqrt{\hbar\omega-\hbar\omega_{\text{con}}}. \tag{27}$$

It resembles the simple DOS expression valid for a parabolic band of a bulk semiconductor. Although we consider nanoclusters of TiO_2 which DOS should differ from this simple type, the expression [Eq. (27)] allows us to clearly indicate the effect of a frequency-dependent DOS. We also calculated spectra with a DOS like that obtained in Refs. 13 and 14 (nearly Gaussian shaped). The obtained differences, however, are so small that they are not interesting enough to be further discussed. All computations presented in the following are based on solutions of Eqs. (7) and (8) with complete consideration of the overlap expressions $\langle\mathcal{N}V_e u_p\rangle_\omega$ between the expansion basis functions u_p and the DOS (the transfer coupling has been replaced by the mean value $\bar{V}_e$).

To notice the dependence of the absorbance on the concrete form of the DOS also in a case where a midband injection position is considered compare the dotted curve of the upper panel in Fig. 8 with that of Fig. 9. (To avoid overloading of the paper we did not present a separate figure.) The upper curves correspond to the DTB–Pe–COOH–TiO_2 system considered so far but in Fig. 9 with a DOS like in Eq. (27) (cf. also Fig. 10). Indeed, the frequency dependence of the DOS moves the absorbance maximum about 0.07 eV below the injection position at $\hbar\varepsilon_e=2.79$ eV.

Such a behavior has to be expected when considering the real part [Eq. (24)] of the self-energy for different DOS. In the case of a frequency-independent DOS a negative value of $\text{Re}\,\Sigma$ follows which results in such a value that in combination with the level broadening the absorbance peak nearly

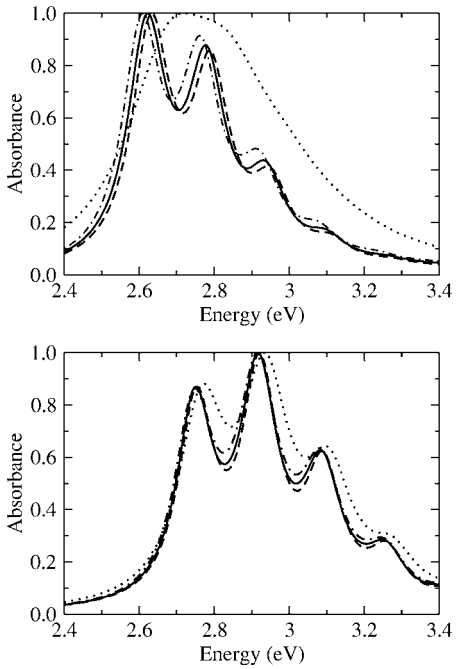

FIG. 9. Rescaled linear absorption spectra of the DTB–Pe–COOH system at the TiO_2 surface (upper panel, dotted line) and the DTB–Pe–$(CH_2)_2$–COOH system at the TiO_2 surface (lower panel, dotted line) and for the frequency-dependent DOS of Eq. (27) (lower band edge at 1.79 eV). To indicate the effect of an injection position closer to the band edge than in TiO_2, curves with an increasing band edge are also shown. Dashed-dotted line: $\hbar\omega_{\mathrm{con}}=2.69$ eV, solid line: $\hbar\omega_{\mathrm{con}}=2.79$ eV, and dashed line: $\hbar\omega_{\mathrm{con}}=2.89$ eV. (To be comparable with the spectra of Fig. 8 the DOS $\mathcal{N}/\hbar$ has to be normalized to 2/eV in different energy intervals above the band edge: [0.8,1.8 eV] for $\hbar\omega_{\mathrm{con}}=1.79$ eV, and [0,1 eV] for $\hbar\omega_{\mathrm{con}}=2.69$, 2.79, and 2.89 eV, cf. Fig. 10.)

stays at the position of the solvent case. Taking, however, $\mathcal{N}(\omega)$ like Eq. (27) the negative value of $\mathrm{Re}\,\Sigma$ increases since the negative contributions in the integrand of Eq. (24) dominate over the positive ones.

Note also that the prefactor in Eq. (27) may take the form $\nu=(L^3/2\pi^2)(2m_e^*/\hbar^2)^{3/2}$ if the parabolic band of a bulk semiconductor (with linear extension L and effective electron mass m_e^*) is considered. Using the effective conduction-band mass of TiO_2 (about $1m_e-10m_e$), positioning $\hbar\omega$ at about 1 eV above $\hbar\omega_{\mathrm{con}}$, and setting L equal to 10 nm one obtains $\bar{\mathcal{N}}/\hbar=200/\mathrm{eV}$. For smaller nanostructures with $L=5$ nm it follows $\bar{\mathcal{N}}/\hbar=25/\mathrm{eV}$. As already done in the Tables I and II we again deduce from the broadening $\bar{\Gamma}$ respective mean values of $\bar{V}_e$ but now using the above-mentioned values of $\bar{\mathcal{N}}/\hbar$. For the DTB–Pe–COOH [DTB–Pe–$(CH_2)_2$–COOH] system we get 0.012 eV (0.006 eV) using $\bar{\mathcal{N}}/\hbar=200/\mathrm{eV}$ and 0.034 eV (0.016 eV) when using $\bar{\mathcal{N}}/\hbar=25/\mathrm{eV}$. We consider such values of $\bar{V}_e$ to be unreasonably small, indicating that for the system under consideration a bulk semiconductor DOS is of no use.

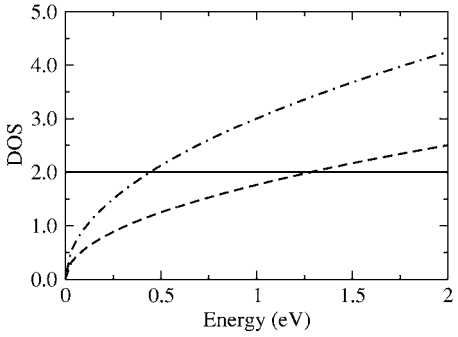

FIG. 10. DOS according to Eq. (27) vs $E=\hbar\omega-\hbar\omega_{\mathrm{con}}$ (shown is $\mathcal{N}/\hbar$). Full line: $\bar{\mathcal{N}}/\hbar=2/\mathrm{eV}$, dotted line: $\mathcal{N}/\hbar$ normalized to 2/eV in the energy interval [0.8,1.8 eV], and dashed-dotted line: normalization within the energy interval [0,1 eV].

VI. CHARGE INJECTION NEAR THE BAND EDGE

The results of the foregoing section are confronted in what follows with the absorption spectra one obtains if the charge injection would take place near the lower band edge. Since no other data are available at the moment we again use the parameters derived for the perylene-TiO_2 system with the only exception that the lower band-edge $\hbar\omega_{\mathrm{con}}$ takes values closer to the excited-state energy of perylene (i.e., we chose $\hbar\omega_{\mathrm{con}}=2.69$, 2.79, and 2.89 eV). Since at the band edge the DOS starts to take finite values (or jumps from zero to its constant value as in the case of $\bar{\mathcal{N}}$) the following considerations also supplement the discussion of the preceeding section.

A. The absorbance spectra

The absorption line shapes of Pe–COOH–TiO_2 as well as of Pe–$(CH_2)_2$–COOH–TiO_2 for such a situation with an upwards shifted band edge are presented in Fig. 8 where a constant DOS has been used, and in Fig. 9 based on the frequency-dependent DOS of Eq. (27). To make the latter results comparable with those obtained with a constant DOS the prefactor ν of Eq. (27) has been defined in the following way. It should take such a value that the averaging within the energy range where the absorbance is different from zero coincides with the values of $\bar{\mathcal{N}}$. This yields for the case of the true TiO_2 band-edge position of 1.79 eV the value $\nu=1.43/\mathrm{eV}^{2/3}$ and for the other values shifted upwards $\nu=2.43/\mathrm{eV}^{2/3}$ (cf. also the caption of Fig. 9). The shape of the two frequency-dependent DOSs compared to the constant quantity $\bar{\mathcal{N}}$ can be found in Fig. 10.

Let us first turn to the constant DOS case [Fig. 8]. Once $\hbar\omega_{\mathrm{con}}$ is moved from the reference position of 1.79 eV to a position of 0.1 eV below the excited dye state (dashed-dotted curve in the upper panel of Fig. 8), the vibrational structure is resolved with the 0-0 transition at about 2.65 eV. This is a low-energy shift of more than 0.1 eV when compared with the solvent case. If $\hbar\omega_{\mathrm{con}}$ is further increased (full and dashed lines of Fig. 8) the 0-0 peak position is slightly shifted to higher energies and the 0-0 transition line becomes larger than that of the 0-1 transition. Such a behavior is to be expected since a further increase of the band-edge position $\hbar\omega_{\mathrm{con}}$ should lead to spectra similar to the solvent case with the 0-0 transition again at 2.79 eV. (Concentrating on the dashed curve in the upper panel of Fig. 8 one considers a case where a part of the overall absorption line is positioned within the band gap.)

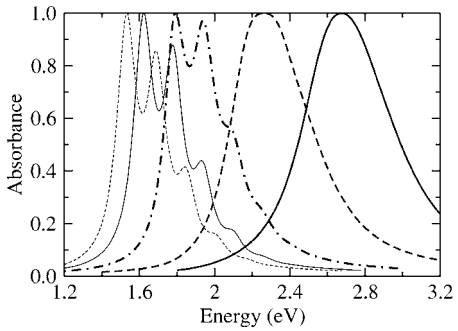

FIG. 11. Rescaled linear absorption spectra of a fictitious molecule at the TiO_2 surface that can change the injection position $\hbar\varepsilon_e$. Solid line: $\hbar\varepsilon_e$ =2.79 eV (corresponding to DTB–Pe–COOH), dashed line: $\hbar\varepsilon_e$=2.39 eV, dashed-dotted line: $\hbar\varepsilon_e$=2.19 eV, dotted line: $\hbar\varepsilon_e$=1.99 eV, thin solid line: $\hbar\varepsilon_e$=1.79 eV, and thin dashed line: $\hbar\varepsilon_e$=1.69 eV (used DOS: dashed-dotted line of Fig. 10).

Of course, the absorption line shift has been induced by the strong-transfer coupling $\bar{V}_e$ (resulting in large values of $\mathrm{Re}\,\Sigma$ and $\mathrm{Im}\,\Sigma$, cf. Eqs. (24) and (18), respectively), which moves the excited dye state downwards. According to the discussion of the foregoing section the (low-energy) shift of the absorbance becomes stronger if the energetic distance between the excited dye levels and the band-edge $\hbar\omega_{\mathrm{con}}$ becomes smaller. If the dye level coincides with or is positioned below $\hbar\omega_{\mathrm{con}}$ the shift decreases (the expression [Eq. (24)] for $\mathrm{Re}\,\Sigma$ lost its singularity). This all is reflected by the curves displayed in the upper panel of Fig. 8 (remember, however, that the concrete computations have been carried out according to the scheme of Sec. III A avoiding the handling of any singular integral). The described behavior is less pronounced for $\mathrm{Pe}-(\mathrm{CH}_2)_2-\mathrm{COOH}-\mathrm{TiO}_2$ (lower panel of Fig. 8). Nevertheless, the line shape deviates a little bit from that of the midband injection position.

Let us now change to the more realistic case of a frequency-dependent DOS as introduced in Eq. (27) and Fig. 10. In the strong-coupling case (upper panel of Fig. 9) we obtain the same behavior as for a constant DOS. For the band-edge position somewhat below the injection level the low-energy shift of the absorbance is maximal (dashed-dotted line in the upper part of Fig. 9). The shift is less pronounced if the position of the band-edge $\hbar\omega_{\mathrm{con}}$ is further shifted upwards (full and dashed lines in the upper panel of Fig. 9). The respective explanation has been already given in relation to the constant DOS case (see above). Since a frequency-dependent DOS has been used which increases continously away from $\mathcal{N}=0$ when increasing ω above ω_{con} the differences between the absorbances for the near-band-edge cases are less pronounced than in Fig. 8. In particular, the 0-0 transition peak is larger than that for the 0-1 transition. The behavior of the absorbance in the case of a somewhat weaker coupling to the band continuum (lower part of Fig. 9) is nearly identical to the case of a constant DOS (lower panel of Fig. 8) and should not be discussed in more detail here.

Finally, to have a comparable sequence of spectra Fig. 11 shows the absorbances for the fixed band-edge position at $\hbar\omega_{\mathrm{con}}$=1.79 eV but with decreasing injection position $\hbar\varepsilon_e$ and the use of a common frequency-dependent DOS (dashed-dotted line in Fig. 10). The spectra display the increasing resolution of the vibrational progression when moving with the injection position $\hbar\varepsilon_e$ near and below the band edge. In any case the maximum of the absorbance is more than 0.1 eV below the respective value of $\hbar\varepsilon_e$ again indicating the effect of the band-continuum-induced shift of the excited electron-vibrational dye levels.

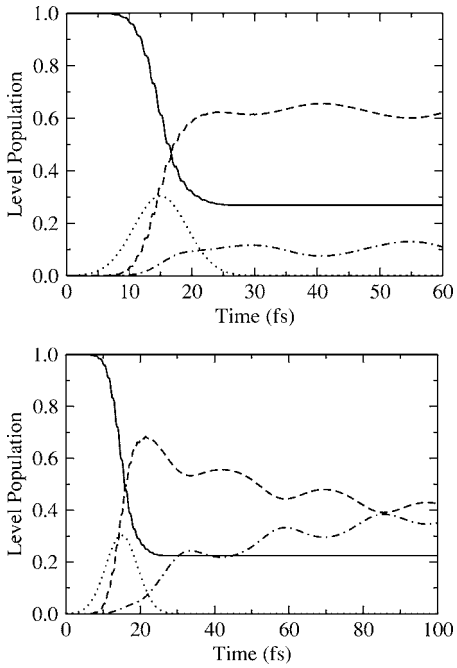

FIG. 12. Electronic level population after a 10 fs (FWHM) laser-pulse excitation of a fictitious molecule at the TiO_2 surface with its charge injection position $\hbar\varepsilon_e$ degenerate with the lower band-edge $\hbar\omega_{\mathrm{con}}$=1.79 eV. Upper panel: other parameters similar to the DTB–Pe–COOH system (see Table I) and lower panel: reorganization energy $\lambda_{\mathrm{ion}\,e}$ for the transition from the excited dye state into the ionized state set equal to 0.36 eV ($Q_{\mathrm{ion}}-Q_e=3$). Solid line: ground-state population P_g of the dye, dashed line: excited-state population P_e of the dye, dashed-dotted line: population P_{ion} of the ionized dye (what equals the total conduction-band population), and dotted line: laser-pulse envelope (in a.u., direct excitation of the 0-0 transition).

B. Charge injection dynamics

Charge injection dynamics for the degenerate case $\varepsilon_e=\omega_{\mathrm{con}}$ are displayed in Fig. 12 (see also the recent studies in Ref. 15). The curves correspond to the case represented by the thin solid line in Fig. 11 and should be confronted with the charge injection dynamics of the midband injection case shown in the upper panel of Fig. 2. First, the positioning at the band edge, roughly speaking, converts the behavior of the excited-state population P_e and that of the band continuum. Now, there is less band continuum population (at about 0.1). However, this value is reached also within about 10 fs. Second, the curve for P_e displays oscillations indicating charge recurrences from the band continuum into the excited dye state. Such a behavior is typical for the near-band-edge positioning of the injecting level.[10] If cases are studied where ε_e is tuned away a little bit from ω_{con} the results look similar (cases shown by the thin full and dashed lines in Fig. 11). So we may conclude that the charge injection dynamics do not change drastically if one moves from a

midband injection position to the near-band-edge case. But in contrast to the case shown in Fig. 2 there is complete electron transfer into the conduction band.

If, however, the reorganization energy $\lambda_{\text{ion }e}$ for the transition from the excited dye state into the ionized state is increased (lower panel of Fig. 12) the charge injection dynamics undergo a rather drastic change. Now, the band continuum population increases (it is stabilized by the rather large value of $\lambda_{\text{ion }e}$) together with an increase of the injection time.

VII. CONCLUSIONS

In the present paper we continued recent theoretical studies on linear absorption spectra related to ultrafast heterogeneous electron transfer (HET) from perylene to nanostructured TiO_2.[11] A time-dependent formulation of the absorbance has been complemented by a frequency-domain description. In this way the linear absorbance as well as the temporal evolution of the sub-100 fs charge injection dynamics were described. The dependence on the reorganization energies of the involved intramolecular transitions has been underlined. The effect of changing the transfer integral which couples the excited dye state to the band continuum has been demonstrated, and the influence of the concrete form of the semiconductor band DOS could be shown.

Particular emphasis was put on the case where the charge injection level of the dye is near or somewhat below the band edge. The results display the change from a structureless absorption to a well-resolved vibrational progression including characteristic shifts of the absorption lines which are a direct measure for the dye-semiconductor coupling. Experiments to confirm these latter predictions are underway.

ACKNOWLEDGMENTS

The financial support by the Deutsche Forschungsgemeinschaft through Sonderforschungsbereich 450 is gratefully acknowledged.

APPENDIX A: THE INJECTION LEVEL GREEN'S OPERATOR

Studying charge injection processes the use of Green's operator projected onto the injecting level, here φ_e, is mandatory. It has been already introduced in Eq. (13). Its appearance is typical for various surface studies (cf., e.g., Ref. 16). The Fourier-transformed expression follows as

$$\hat{G}_e(\omega) = \frac{\hat{\Pi}_e}{\omega - \varepsilon_e - H_e/\hbar - \Sigma(\omega - H_{\text{ion}}/\hbar) + i\epsilon}, \tag{A1}$$

with the self-energy $\Sigma(\omega)$ introduced in Eq. (17). When entering $\hat{G}_e(\omega)$ it has to depend on the vibrational Hamiltonian H_{ion} too.

Matrix elements $G_{e,MN}$ of $\hat{G}_e$ taken with respect to vibrational states χ_{eM} of the excited dye state can be deduced from the following equation:

$$\langle \chi_{eM} | (\omega - \varepsilon_e - H_e/\hbar - \Sigma(\omega - H_{\text{ion}}/\hbar)) \hat{G}_e(\omega) | \chi_{eN} \rangle = \delta_{M,N}. \tag{A2}$$

It results in

$$(\omega - \varepsilon_e - \omega_{eM}) G_{e,MN}(\omega) - \sum_K \langle \chi_{eM} | \Sigma(\omega - H_{\text{ion}}/\hbar) \times | \chi_{eK} \rangle G_{e,KN}(\omega) = \delta_{M,N}, \tag{A3}$$

with the self-energy matrix elements,

$$\langle \chi_{eM} | \Sigma(\omega - H_{\text{ion}}/\hbar) | \chi_{eK} \rangle = \sum_L \langle \chi_{eM} | \chi_{\text{ion }L} \rangle \Sigma(\omega - \omega_{\text{ion }K}) \times \langle \chi_{\text{ion }L} | \chi_{eK} \rangle. \tag{A4}$$

There are two limiting cases resulting in a simple expression for $G_{e,MN}(\omega)$. First, let us assume that the reorganization energy for the charge injection is small. Then, we may conclude $\langle \chi_{\text{ion }L} | \chi_{eK} \rangle \approx \delta_{L,K}$ what results in $\langle \chi_{eM} | \Sigma(\omega - H_{\text{ion}}/\hbar) | \chi_{eK} \rangle \approx \delta_{M,K} \Sigma(\omega - \omega_{\text{ion }M})$ and, thus, in

$$G_{e,MN}(\omega) = \frac{\delta_{M,N}}{\omega - \varepsilon_e - \omega_{eM} - \Sigma(\omega - \omega_{\text{ion }M}) + i\epsilon}. \tag{A5}$$

A similar expression is found in the framework of the so-called *wide-band* approximation where any frequency dependence of the self-energy is neglected. Replacing Σ in Eq. (A4) by the frequency-independent expression $\bar{\Sigma}$, Eq. (A5) is reproduced. But the frequency-dependent self-energy has been substituted by $\bar{\Sigma}$.

APPENDIX B: STANDARD DESCRIPTION OF LINEAR ABSORPTION

Computing linear absorption spectra of molecular systems represents a standard task (cf., e.g., Ref. 17) and is based on the following expression:

$$\alpha(\omega) = \frac{4\pi\omega n_{\text{mol}}}{\hbar c} \text{Re} \int_0^\infty dt e^{i\omega t} \times \langle \text{tr}\{\hat{W}_{\text{eq}}[\hat{\mu}(t), \hat{\mu}]_-\} \rangle_{\text{disorder}}. \tag{B1}$$

It relates the frequency-dependent absorbance to the half-sided Fourier-transformed dipole-dipole correlation function. Here, n_{mol} denotes the volume density of the absorbing dye, and the thermal equilibrium state of the dye-semiconductor system before photoabsorption is characterized by the statistical operator $\hat{W}_{\text{eq}}$. The time dependence of the dipole operator $\hat{\mu}(t)$ has been induced by the Hamiltonian $H_{\text{M-S}}$ [Eq. (1)]. Averaging with respect to structural and energetic disorder was also introduced, symbolized by $\langle \cdots \rangle_{\text{disorder}}$. In the following we only account for random orientation of the dyes (leading to the well-known prefactor 1/3). Since non-Condon effects are of less importance for our further treatment we introduce the combined DOS $\mathcal{D}_{\text{abs}}$. It enters the absorption according to

$$\alpha(\omega) = \frac{4\pi^2 \omega n_{\text{mol}}}{3c} |\mathbf{d}_{eg}|^2 \mathcal{D}_{\text{abs}}(\omega), \tag{B2}$$

and takes the following form:

$$\mathcal{D}_{\mathrm{abs}}(\omega) = \frac{1}{\pi\hbar}\,\mathrm{Re}\int_0^\infty dt e^{i\omega t} \times \mathrm{tr}_{\mathrm{vib}}\{\langle\varphi_e|(\mathcal{U}_{\mathrm{M\text{-}S}}(t)[\hat{r}_g|\varphi_e\rangle \times\langle\varphi_g|])|\varphi_g\rangle\}. \tag{B3}$$

Here, the trace with respect to the vibrational states is denoted by $\mathrm{tr}_{\mathrm{vib}}\{\cdots\}$, and time evolution follows from the superoperator $\mathcal{U}_{\mathrm{M\text{-}S}}(t)$. Moreover, Eq. (B3) neglects antiresonance contributions (resonances at negative frequencies) and assumes that $\hat{W}_{\mathrm{eq}}$ describes vibrational equilibrium in the electronic ground state, i.e., $\hat{r}_g|\varphi_g\rangle\langle\varphi_g|$. If expanded with respect to the vibrational eigenstates χ_{gN} of the vibrational Hamiltonian H_g the density operator of the vibrational equilibrium is given by $\hat{r}_g = \Sigma_N f(\hbar\omega_{gN})|\chi_{gN}\rangle\langle\chi_{gN}|$ (f is the respective thermal distribution).

Because a direct account for dissipative effects will not be undertaken the action of $\mathcal{U}_{\mathrm{M\text{-}S}}(t)$ reduces to the application of $\exp(-iH_{\mathrm{M\text{-}S}}t/\hbar)$ from the left and the Hermitian conjugated version from the right. It yields

$$\mathcal{D}_{\mathrm{abs}}(\omega) = -\frac{1}{\pi\hbar}\,\mathrm{Im}\int dt e^{i(\omega+\varepsilon_g)t}\mathrm{tr}_{\mathrm{vib}}\{\hat{r}_g e^{iH_g t/\hbar}\hat{G}_e(t)\}, \tag{B4}$$

with Green's operator introduced in Eq. (13). If the coupling to the conduction band is neglected the standard relation for $\mathcal{D}_{\mathrm{abs}}$ is obtained (cf., e.g., Ref. 17).

[1] B. O'Regan and M. Grätzel, Nature (London) **353**, 737 (1991).
[2] R. J. D. Miller, G. McLendon, A. Nozik, W. Schmickler, and F. Willig, *Surface Electron Transfer Processes* (VCH, New York, 1995).
[3] J. B. Asbury, E. Hao, T. Wang, H. N. Ghosh, and T. Lian, J. Phys. Chem. B **105**, 4545 (2001).
[4] J. Kallioinen, G. Benkö, V. Sundström, J. E. I. Korppi-Tommola, and A. P. Yartsev, J. Phys. Chem. B **106**, 4396 (2002).
[5] A. Hagfeldt and M. Grätzel, Chem. Rev. (Washington, D.C.) **95**, 49 (1995).
[6] K. Schwarzburg, R. Ernstorfer, S. Felber, and F. Willig, Chem. Rev. (Washington, D.C.) **248**, 1259 (2004).
[7] S. Ramakrishna, F. Willig, and V. May, Phys. Rev. B **62**, R16330 (2000).
[8] S. Ramakrishna, F. Willig, and V. May, Chem. Phys. Lett. **351**, 242 (2002).
[9] S. Ramakrishna, F. Willig, V. May, and A. Knorr, J. Phys. Chem. B **107**, 607 (2003).
[10] L. Wang and V. May, J. Chem. Phys. **121**, 8039 (2004).
[11] L. Wang, R. Ernstorfer, F. Willig, and V. May, J. Phys. Chem. B **109**, 9589 (2005).
[12] L. Gundlach, S. Felber, W. Storck, E. Galoppini, Q. Wie, and F. Willig, Res. Chem. Intermed. **31**, 39 (2005).
[13] P. Persson, R. Bergström, and S. Lunell, J. Phys. Chem. B **104**, 10348 (2000).
[14] P. Persson, M. J. Lundqvist, and A. Borg (unpublished).
[15] W. R. Duncan, W. M. Stier, and O. V. Prezhdo, J. Am. Chem. Soc. **127**, 7941 (2005).
[16] M. Cizek, M. Thoss, and W. Domcke, Phys. Rev. B **70**, 125406 (2004).
[17] V. May and O. Kühn, *Charge and Energy Transfer Dynamics in Molecular Systems* (Wiley-VCH, Berlin, 2004).